A REALISTIC MODEL FOR POINT-SOURCES IMAGED ON ARRAY DETECTORS: THE MODEL AND INITIAL RESULTS

W.J. MERLINE[†] and STEVE B. HOWELL

Planetary Science Institute
620 N. 6th Ave.
Tucson, AZ 85705

ABSTRACT

We have constructed a computer model for simulation of point-sources imaged on two-dimensional detectors. An attempt has been made to ensure that the model produces "data" that mimic real data taken with 2-D detectors. To be realistic, such simulations must include randomly generated noise of the appropriate type from all sources (*e.g.* source, background, and detector). The model is generic and accepts input values for parameters such as pixel size, read noise, source magnitude, and sky brightness. Point-source profiles are then generated with noise and detector characteristics added via our model. The synthetic data are output as simple integrations (one-dimensional), as radial slices (two-dimensional), and as intensity-contour plots (three-dimensional). Each noise source can be turned on or off so that they can be studied separately as well as in combination to yield a realistic view of an image. This paper presents the basic properties of the model and some examples of how it can be used to simulate the effects of changing image position, image scale, signal strength, noise characteristics, and data reduction procedures.

Use of the model has allowed us to confirm and quantify three points: 1) The use of traditional-size apertures for photometry of faint point-sources adds substantial noise to the measurement which can significantly degrade the quality of the observation; 2) The number of pixels used to estimate the background is important and must be considered when estimating errors; and 3) The "CCD equation" normally used by the astronomical community consistently *overestimates* the signal-to-noise obtainable by a measurement while a revised equation, discussed here, provides a better estimator.

"... so as far as I can see at present, knowledge is nothing but perception."

"Indeed, it is now perfectly plain that knowledge is something different from perception."

Theaetetus to Socrates
Sections 151E and 186E of
Plato's *Theaetetus* (c. 368 BC)

[†] Also Lunar and Planetary Lab, University of Arizona, Tucson AZ 85721

1. INTRODUCTION

The use of two-dimensional (2-D) digital detectors, such as charge-coupled-devices (CCDs), for observational research is the standard throughout the astronomical community. Widely available image processing packages used in astronomy (*e.g.* IRAF, MIDAS, AIPS) contain provisions to manipulate data collected using such detectors. These packages consist of many general purpose routines for doing a wide variety of analyses and some even have provisions for producing artificial data. Specific programs, such as DAOPHOT (Stetson 1987) and IRAF/ARTDATA are worthy of special mention here; not only are they part of the general class listed above, but they contain software that can produce artificial point-sources based on modeling of real data made available to the software. The above packages are being used by an increasing number of astronomers and they work quite well.

For applications to 2-D or aperture photometry of point-sources, the available software ranges from adequate to extremely complex. There are some situations, however, for which these packages are not suited. This is not to be taken as a criticism, since they were never intended to work in such specialized regimes as low signal-to-noise (S/N) or undersampled data. In this paper we present a simple software model; we intend it to be used to study the problems associated with imaging of point-sources in both normal and many of the specialized cases mentioned above.

Much previous work has been done to better understand point-sources imaged on detectors and to examine how one determines the S/N and accuracy of such measures. King (1971), for example, assembled data from various sources and showed the true profile of a stellar image. The effects of seeing on point-sources was discussed in great detail by Young (1974). With the widespread use of digital detectors, many other papers have appeared, at varying levels of complexity, aimed at exploring and understanding properties such as S/N, pixel size *vs.* observational program, imaging of moving objects, stellar photometry, and A/D converters (*e.g.*, Nather 1972; Adams *et al.* 1980; McMillan and Stoll 1982; Djorgovski 1984; Jayroe 1984; Jayroe and Schroeder 1984; Stetson 1987; Howell *et al.* 1988; Gilliland and Brown 1988; Opal 1980; Buonanno and Iannicola 1989; Stone 1989; Jacoby 1990; Philip *et al.* 1990; Kjeldsen and Frandsen 1992; Howell 1993; references therein and other citations within this paper). In particular, Newberry (1991) (hereafter NEWB91) gives a complete description of signal-to-noise considerations for CCD photometry and

the errors associated with data reductions. Our approach parallels his, although in this paper we also derive error expressions for clarity and completeness. We have benefitted from the above-listed works and from personal discussions with many of the authors, for which we are thankful. Many of the previous "idealized" models developed by the community provided some of the ideas we used as starting points for our own work.

What seemed to be missing was a simple, yet accurate, software package that would allow calculation of realistic models of point-sources for a wide range of input conditions. We therefore saw the need within the community, as well as for our own special research needs, to develop such a model. In the process, we have made an effort to make the model flexible enough so that it can be of general use to astronomers seeking to optimize observations of point-sources. Using the model, an observer can realistically and quantitatively evaluate the relative merits of using different telescope/instrument packages. With the stiff competition for telescope time, especially dark time on large telescopes, it is imperative that observers have a means of assessing how the data quality will be affected by changes in telescope aperture, filter used, detector characteristics, or lunar phase. In addition, this type of modeling can be used to simulate the effects of various reduction techniques (see, *e.g.*, Howell 1990a,b; Stetson 1990a,b).

As examples, we have sucessfully applied the model to optimization of detectors for a survey of night sky brightness and have used it to determine the best methods of observing very bright objects with large telescopes — in this case for obtaining extreme sensitivity to faint flashes on the limb of Jupiter and from the Galilean satellites during the impact of comet Shoemaker-Levy 9 (Howell and Merline 1995).

Our software calculates a realistic model of a user-determined point-source imaged onto a CCD. It *does not* take, as input, raw or reduced CCD frames and reduce or analyze them, since it is not intended to be a data reduction facility. The model is simple to use — all input is via one ASCII file. This file (see Table 1) serves as a template that is simply "filled in", which gives the user complete control, without ambiguity, over inputs that are easy to understand. The program then reads the current values from this file and calculates the desired model. We designed and wrote the FORTRAN software to be used on a PC/AT-class machine so that it could be widely available to the community. It runs as a stand-alone program and so can be used independent of larger software

packages and without the necessary understanding of many manuals of documentation. A typical 3-D model is calculated in under 30 seconds.

We wanted the code to run quickly to allow us to use it interactively or test the statistical properties of the model by repetition, but we also wanted it to be as accurate as possible. This is just as important as speed if one is going to use the output to gain insight into understanding how point-sources are imaged onto CCDs. We apply these models to our own research interests and also intend them to be used to develop better techniques of data reduction, which can then be incorporated into larger general software packages or aid those who want to explore in detail the nature or even the subtleties of 2-D imagery. The model can also be used to assess the performance of various CCDs for specific applications, thereby assisting in planning for observations.

Examples of applications of the program and our initial results are presented after the description of the model. These are slightly biased toward our research interests (time-series and differential photometry of point-sources at low S/N, "fuzzy" objects, and spacecraft imagery) but, as will be shown, the software is flexible and easily can be adapted and used by others for their own favorite applications and specific observing strategies. We call the model realistic because we have included most relevant noise sources associated with these types of observations both in the star and background, and in the detector. The model yields a 3-D (x, y, intensity) grid of all noise sources, equivalent to that "seen" by the users' CCD system.

Section 2 presents the model in detail both for completeness and, we hope, for interest to those who want to follow the derivation of the "standard" equations (see also NEWB91). We show some of the ways the model can be used and then give some initial results in Section 3. At the end of the paper, we discuss our conclusions and future directions.

2. THE MODEL

Our objective is to make the model simulate a real instrument as closely as possible. This means that not only the detector and light source must be realistic, but that all (normally present) sources of noise that appear in real data must be included and properly characterized in the model. Furthermore, observer-dependent factors such as pixel binning and background subtraction must be addressed.

Because of the relevance of point-sources and the widespread use of CCDs, we chose to model an astronomical point-source imaged on a two-dimensional detector. Our initial model is intended only for *point-sources*, with applications to spectroscopy or extended sources, for example, to be addressed in the future.

Just as in a real instrument, we "expose" our detector to the "light" of a point-source broadened appropriately for seeing, the distribution of energy being determined by a point spread function. Each pixel independently collects "light" from each of the usual generators of photoelectrons (source, sky, dark) and contains a bias "signal" as well. Random noise of the appropriate type is added to each of these sources of signal on a pixel-by-pixel basis. The photometric integration is a simple sum, corrected for background, over a circular aperture. For the models we present here, background determination is done as a simple average of pixels taken from a "background" array.

The model accepts input values for parameters such as pixel size, read noise, source magnitude, and sky brightness (see Table 1 for a complete list of input parameters and brief description). Each noise source can be turned on or off so that they can be studied separately as well as in combination to yield a realistic view of an image. The synthetic data can be output as simple integrations (one-dimensional), as radial slices (two-dimensional), and as intensity-contour plots (three-dimensional).

2 A. FLUX CALIBRATION

If we are to use the model to simulate actual stellar observations, we must calibrate the model's input flux with that expected from a specified source under given environmental and instrumental conditions. Of course, there are several factors that determine the flux recorded by our detector. For clarity and ease of use, we include explicitly each independent factor where possible.

Given the brightness of the source and its spectral type, the absolute flux $F(\lambda)$, in erg cm^{-2}s^{-1}Å^{-1}, outside the earth's atmosphere and within a certain bandpass ($\Delta\lambda = \lambda_2 - \lambda_1$), can be determined. A correction factor $E(\lambda)$ for extinction due to the airmass associated with the observation, as well as the areas of the telescope aperture A and secondary obstruction a are included explicitly. Transmission of the filter is $T(\lambda)$. The remainder of the optical system, however, is treated simply by having one optical efficiency factor $\epsilon(\lambda)$ that characterizes the entire train. The energy flux is then converted to the rate of arrival of detected photons C, using the quantum

efficiency $Q(\lambda)$ of the detector, as follows:

$$C = \int_{\lambda_1}^{\lambda_2} F(\lambda) \left(\frac{\lambda}{hc}\right) (A-a)\,\epsilon(\lambda)\,T(\lambda)\,E(\lambda)\,Q(\lambda)\,d\lambda \quad . \tag{1}$$

For the above parameters, the current version of the program uses averages over the bandpass, rather than integrating, such that the detected count rate is

$$C = \bar{F}\,\frac{\bar{\lambda}}{hc}\,(A-a)\,\bar{\epsilon}\,\bar{E}\,\bar{Q}\,\Delta\lambda \quad , \tag{2}$$

where $T(\lambda)$ has been incorporated into $\bar{\epsilon}$ and $\Delta\lambda$, and the average flux $\bar{F}$ (for the selected spectral type and magnitude) and atmospheric transmission are calculated by interpolation of tabular data, included from Allen (1973).

2 B. MODEL DETECTOR AND OPTICAL CONFIGURATION

The model simulates a CCD detector exposed to visible light. The CCD is characterized by only a few parameters (see Table 1). Quantum efficiency and pixel size govern the detection rate of photoelectrons per resolution element, while read noise and gain determine the non-shot noise components. Bias level is largely inconsequential; it appears here so that model output can look numerically similar to real raw data.

For the examples given later in this paper we have modeled detectors and telescopes similar to those available at National Optical Astronomy Observatories (NOAO) / Kitt Peak National Observatory (KPNO). The Kitt Peak CCD systems have been used as sources of both observational data for comparison and as well-characterized systems with values we could input for our tests. The quantum efficiencies we use are averages over the chosen bandpass and are taken from KPNO operating manuals and newsletters. Estimates for the optical efficiency parameter will, of course, depend on the condition of the telescope mirrors, the transmission of the filter, and the number of other optical surfaces encountered by the beam. The value is most easily determined from actual measurements. Therefore, we have worked backward by using real observations to estimate this efficiency. For the models here, ϵ has turned out to be a reasonable value, about 50%.

2 C. POINT SPREAD FUNCTION

King (1971) and Young (1974) showed that the point spread function (PSF) of a stellar image, observed with a ground-based telescope, is only approximately Gaussian. Therefore, we do not use a Gaussian function for our model. Instead, we use a function that was constructed by fits to actual 2-D images of astronomical point-sources, including typical smearing effects of seeing, guiding, and telescope optics. The PSF chosen, which is approximately Lorentzian in shape, is that discussed by Diego (1985). The function, yielding the relative intensity I at any point (x, y) in the image, is reproduced below directly from Diego:

$$I(x, y) = \frac{1}{1 + d_1^{p(1+d_2)}} \quad , \tag{3}$$

where

$$d_1 = \sqrt{\left(\frac{x}{r_x}\right)^2 + \left(\frac{y}{r_y}\right)^2} \quad \text{and} \quad d_2 = \sqrt{\left(\frac{x}{p_{rx}}\right)^2 + \left(\frac{y}{p_{ry}}\right)^2} \tag{4}$$

and r_x and r_y are radii along the x and y directions; p_{rx} and p_{ry} are scale factors which modify the exponent p. The numerical values for each of these parameters, as determined by fits to real stellar data, are given in the form of plots by Diego. The parameters are all functions of the full width at half-maximum (FWHM) of the image.

For simplicity, we use only radially symmetric images. Equation (3) can then be recast in the following form:

$$I(r) = \frac{1}{1 + \left(\frac{r}{r_0}\right)^{p\left[1 + \frac{r}{p_r}\right]}} \tag{5}$$

where now I is the intensity at the radial coordinate r of the PSF; r_0 is the radius (HWHM) of the PSF; p and p_r (where $p_r = p_{rx} = p_{ry}$) are the fitted parameters taken directly from Diego.

In general, the function appears Lorentzian near the peak, but the modified exponent forces the function to decrease faster than Lorentzian as the distance from the peak increases. It also has the feature that sharper images have a larger fraction of the light concentrated near the peak than one would get by using a pure Lorentzian function. We normalize the PSF by determining the amplitude A_0 such that the integral of the normalized PSF over the entire image matches the requested count rate C (see Equation 2) from the source:

$$A_0 \int_0^\infty 2\pi r I(r)\, dr = C \quad . \tag{6}$$

2 D. CONSTRUCTION AND INTEGRATION OF IMAGES

The first step in the process of integrating the signal from an image is the selection of the pixels to be used. We define our integration window to be a circular aperture that is usually, but need not be, centered on the center of the image of the star. This allows one to study the effects of errors in centering of the integration window. The radius of the aperture (in terms of FWHM of the image) is an input to the program. Near the edge of the circular aperture, we have the inevitable problem of rectangular pixels that lie partially outside the integration area. Any pixel having its geometric center inside the edge of the aperture is included in the integration; any pixels that do not meet this criterion are rejected.

The detected level of analog signal on each pixel is the result of a combination of signals having four distinct origins: the source itself (the star), the background level (or sky), the dark signal, and the DC bias (offset). The average bias, dark, and sky levels are input by the user and are assumed to be constant over the detector. Since the source intensity is a function of distance r from the image center, we perform a two-dimensional integration of the normalized PSF ($A_0 I(r)$; Equations 5 and 6) over each pixel individually.

Random noise of the appropriate type must be added to each of the four "signal-generating" processes above, on a pixel-by-pixel basis. This procedure is discussed in Section 2F. Thus, we generate a signal in much the same way as it is generated in a real detector. Having the noise introduced in this way allows errors to propagate themselves along in the integration and reduction process. The result can be compared with the formal, analytical error propagation which is discussed in Section 2G.

The total integrated photometric signal S, in analog-to-digital units (ADU), for a point-source image is given by Equation (7). [Refer to the Appendix for definitions of parameters used here and in subsequent equations.]

$$S = \sum_{i=1}^{n_{pix}} (I_i^\star + I_i^D + I_i^S + I_i^O) - n_{pix}\bar{B} + n_{pix}\bar{d} \tag{7}$$

We sum over all the pixels n_{pix} in the aperture and correct for the background level $\bar{B}$ and a digitization offset $\bar{d}$, which are discussed below. Before performing the integration over all pixels, we must first sum the contributions, within each pixel, from the four components discussed above.

Accompanying this, as in a real instrument, is the subsequent loss of information about the origin of any particular photoelectron. Letting I_i equal this sum for any pixel i, Equation (7) becomes:

$$S = \sum_{i=1}^{n_{pix}} I_i - n_{pix}\bar{B} + n_{pix}\bar{d} \quad .$$

(8)

As it must be, the number of photoelectrons contributing to each of I_i^*, I_i^P, and I_i^S is quantized. This is ensured by allowing a Poisson noise generator (discussed in Section 2F) to operate on these quantities at the electron level (*i.e.*, *before* conversion to ADU). I_i^O is typically an analog voltage setting and so is not quantized in the model. The addition of the four components is also done at the electron level, again as in a real instrument. The sum of these four components must then be converted to a data number; therefore, the value $(\sum(I_i^* + I_i^P + I_i^S + I_i^O))$ is rounded to the nearest ADU.

The last term in Equation (8) is the net effect of this conversion from electrons to ADU. In the process, a digital approximation is made of the analog signal from both the stellar and background arrays. In an idealized A/D converter, under most observational circumstances, the average fractional ADU lost (or gained) per pixel $\bar{f}^*$ in the stellar array is the same as that lost/gained in the background array $\bar{f}^B$, such that $\bar{d} = (\bar{f}^* - \bar{f}^B) = 0$; however, the uncertainty in the determination of $\bar{d}$ is *not* zero. For simplicity, therefore, we set $\bar{d} = 0$ here and defer more detailed discussion of $\bar{d}$ and $\sigma_{\bar{d}}$ until Sections 2F and 2G, so

$$S = \sum_{i=1}^{n_{pix}} I_i - n_{pix}\bar{B} \quad .$$

(9)

2 E. BACKGROUND DETERMINATION AND SUBTRACTION

Once we have created a model image, we must make a determination of the average background "beneath" the image of the star, just as must be done for a real observation. Because we cannot identify the origin of individual electrons contributing to the overall raw signal, we must estimate the background level from either another image that does not contain the star, or from the same image but in a part of the CCD that contains "only" background. The "background" here means the average amount of the raw signal per pixel that would be present in the absence of the star. It consists of the sum of the contributions from the bias, the dark signal, and the sky brightness.

Our average background per pixel is determined by producing another image having characteristics identical to the stellar image, but with the star switched off. This is an independent and random determination, so the count will not be identical to the background count "under" the star image, either pixel-by-pixel or in its entirety. In our initial model, the background level is computed using the arithmetic mean of the pixels in the background array. Others may prefer to use a median, mode, or another statistical treatment; they are easily implemented into our software. Howell (1989) discusses methods of background determination for CCD photometry. Equation (10) gives the recipe for this average background:

$$\bar{B} = \frac{1}{n_B} \sum_{j=1}^{n_B} I_j = \frac{1}{n_B} \sum_{j=1}^{n_B} (I_j^D + I_j^S + I_j^O) \quad . \tag{10}$$

The j subscript indicates that the pixels are taken from a separate "sky" array. The summation is over n_B background pixels in this sky array. The user must specify the number of pixels to be used in this array. It is neither necessary nor desirable to have $n_B = n_{pix}$. As pointed out by NEWB91 and shown again here in Section 2G, the error in photometry of a point-source depends on the number of background pixels used. This source of error seems to be often overlooked in photometric reductions. Again, I_j^D and I_j^S are each quantized at the electron level; $\sum (I_j^D + I_j^S + I_j^O)$ is digitized (rounded) at the ADU level.

2 F. CHARACTERIZATION OF NOISE SOURCES

There are five sources of noise treated in the model: photon statistics in the signal from the source, photon statistics in the signal from the sky, noise in the dark level, readout noise, and noise resulting from digitization of the data. We have not yet included fixed-pattern or "scene" noise (Janesick, Hynecek, and Blouke 1981). This limitation to our present code is further discussed in Section 2I.

The digitization noise is introduced into the data simply by operating on the data in a fashion consistent with the quantized nature of the photoelectrons and the conversion from an analog signal to digital values. For all other noise sources, however, the noise must be introduced explicitly. For each pixel and each noise source independently, this is done by drawing from a random distribution (of the appropriate type) about the expected mean count of electrons for a particular exposure.

The initial seeds themselves are determined by the computer clock and are thus taken randomly from a pool of ~65,000 values. Therefore, unless requested, successive runs will not produce identical images. The codes for generation of random numbers were adapted from those of Press *et al.* 1986. Software drivers access these routines, which in turn access intrinsic clock routines contained within *Microsoft* ⊕ FORTRAN, to provide initial seed randomization. Multiple runs can be used as an external check on the validity of the formal (internal) error calculations (given in Section 2G).

As described in Section 2D, the normalized PSF, $A_0I(r)$, integrated over a pixel, determines the count rate of photoelectrons due to the star alone on that pixel. The time-integrated count for that pixel is used as the expected mean value of the stellar signal from that pixel. Noise is imposed such that successive runs of the model (with the same input characteristics) would yield, for each pixel, a Poisson distribution of values about its expected mean.

Poisson sky noise is introduced in a manner identical to that used for the photon statistics in the star signal. In this case, however, the expected mean sky count comes from the user-input sky brightness and exposure time. The sky brightness is input in magnitudes per square arcsec and is converted to counts/pixel/second using the supplied values of the image scale, pixel size, optical efficiency, and quantum efficiency. Given the dark count rate, the dark noise is produced in a similar fashion.

Read noise is treated as Gaussian noise about the bias level. The value input as the read noise, in electrons/pixel/read, is taken as the dispersion of the Gaussian distribution. This noise is introduced into both star and background integrations, before conversion to data numbers, on a pixel-by-pixel basis. Treating the read noise as Gauassian is appropriate for "good data" (Massey and Jacoby 1992), although read noise is the result of many different contributions (Janesick *et al.* 1984) and, therefore, the distribution may deviate somewhat from Gaussian for a particular CCD.

Only integral numbers of electrons can be generated from each source of photoelectrons (sky, star, and dark). Although our stellar energy distribution function $I(r)$ (Equation 5) is smoothly varying over the CCD, the Poisson generator yields discrete values. The generator automatically introduces the correct Poisson noise into our data; we account for this in the analytical error expressions of Section 2G by using the standard expression for the uncertainty in detecting an

average of n photoelectrons, $\sigma_n = \sqrt{n}$. The same process is applied to each of the other sources of photoelectrons, since each one contributes independently to the raw integration on that pixel.

Another source of noise is that inherent in the conversion from analog to digital output. In an ideal A/D converter, the first transition (0 to 1 ADU) will occur at the analog-equivalent of $+\frac{1}{2}$ LSB (least-significant bit); transitions will occur at steps of 1 LSB thereafter. For example, a 3-bit A/D at 10 V full scale (FS) will have 8 steps. One LSB will be equivalent to $\frac{1}{8}$ FS (or 1.25 V). The transitions will occur at $\frac{1}{2}, \frac{3}{2}, \frac{5}{2}$, etc. of this value. Thus, the first transition will be at $\frac{1}{16}$ FS or 625 mV, the others at 1.875 V, 3.125 V, etc. The ideal converter, then, rounds to the nearest ADU any fractional part of the signal "left over" in each pixel after the conversion to an integral number of ADU. Therefore, we may gain or lose up to $\frac{1}{2}$ ADU in each pixel.

Most converters are not ideal and there are many complications associated with the conversion process that ultimately we would like to address. Aside from the quantization, we have A/D zero-point offset error (the step sizes remain fixed, but the transition points are all uniformly shifted), in which the first transition occurs at a point other than $+\frac{1}{2}$ LSB. We can also have scale-factor (gain) error. Here the span between transitions is not (the analog-equivalent of) 1 LSB; in the example above, step spacing would be less or more than the expected 1.25 V. There can be differential linearity error (non-constant A/D step size), populating some A/D levels more than others, even for a uniform distribution of scene brightness levels. If this error is large, some of the A/D codes may be missed entirely, leading to weakly- or un-populated A/D levels (sticky bits). The operation of A/D converters and associated errors are discussed in some detail by Sheingold 1972; Opal 1988 provides a good discussion of A/D converters useful for digital photometry.

We have not, at this point, incorporated all of these effects into our model. In particular, scale and differential linearity errors are highly dependent upon the specific A/D used and, without a proper framework in which to parameterize converters in a general way, we feel that we would add non-existent noise to certain systems, while still leaving out some noise sources in others. We can include those effects that we can reliably characterize, namely the quantization itself and offset error, which are common to *all* A/D converters.

For our models we treat the fractional count per pixel f as being uniformly distributed on the interval $(-\frac{1}{2}, \frac{1}{2})$ and therefore have $\bar{f} = 0.0$ ADU $\pm \sigma_f$. In the presense of offset error, $\bar{f}$ would not necessarily be zero. One would expect this to be significant when attempting accurate photometry.

In general, however, the fractional count lost or gained per pixel in the stellar integration is automatically compensated because the average background per pixel is also over- or under-estimated, by the same fractional count. This compensation is *independent* of the number of pixels in either the background or stellar arrays. There should not be any systematic offset due to the digitization; thus, we have

$$\bar{d} = (\bar{f}^* - \bar{f}^B) = 0 \pm \sigma_{\bar{d}} \quad . \tag{11}$$

This holds only if we assume that the distribution functions for f^* and f^B are the *same*. Furthermore, whenever the gain is comparable with the noise level, *i.e.* whenever the noise is not resolved, this compensation does not necessarily occur and systematic errors can be expected.

The extent to which the above compensation is *uncertain* is what we will call *digitization noise*. The standard errors in the means $\bar{f}^*$ and $\bar{f}^B$ are given by

$$\sigma_{\bar{f}^*}^2 = \frac{\sigma_f^2}{n_{pix}} \qquad \text{and} \qquad \sigma_{\bar{f}^B}^2 = \frac{\sigma_f^2}{n_B} \tag{12}$$

where now σ_f is the uncertainty in estimating the true mean of the distribution of f from the fractional count in a single pixel. For f uniformly distributed on $(-\frac{1}{2}, \frac{1}{2})$, the variance will be $\sigma_f^2 = \int_{-\frac{1}{2}}^{+\frac{1}{2}} (f - \bar{f})^2 df$, so $\sigma_f = \sqrt{1/12}$ ADU $\simeq 0.289$ ADU (see also NEWB91). The digitization noise depends on the number of background and stellar pixels used. In most cases the digitization noise is small; whenever the read noise is resolved, the contribution from digitization noise will be only a few percent of that from read noise.

Our model allows for the A/D rounding to be turned on or off. Using this feature, we can run many trials to empirically determine the effect of digitization, both on the magnitude of the integrations themselves (systematic errors) and on their repeatability (random errors, showing the effect of the digitization *noise*). Results of these tests are consistent with our analytical expressions above and the associated claims.

We have seen that the uncertainty in a photometric observation using a CCD depends not only on the photon statistics of the source, but also on the read noise, the sky noise, the noise in the background measurement, and the noise associated with conversion from an analog signal to data numbers. We reiterate that the process of background subtraction itself is noisy and that uncertainty in the integrations will depend on the number of both background and source pixels used.

2 G. FORMAL ERROR PROPAGATION

In this section we outline the formal propagation of errors for point-source photometry using CCDs. For clarity, all calculations are done in units of electrons rather than ADU. We begin in the standard fashion (see Bevington 1969 or Bottaccini 1975) by expanding the expression for the integrated signal $S = \sum I_i - n_{pix}\bar{B} + n_{pix}\bar{d}$ (Equation 8) into a Taylor series about the mean value $\bar{S}$. We then take as a measure of the width of the distribution of $(S - \bar{S})$ the variance

$$\sigma_S^2 = \sum_{i=1}^{n_{pix}} \left(\frac{\partial S}{\partial I_i}\right)^2 \sigma_{I_i}^2 + \left(\frac{\partial S}{\partial \bar{B}}\right)^2 \sigma_{\mathcal{B}}^2 + \left(\frac{\partial S}{\partial \bar{d}}\right)^2 \sigma_{\mathcal{d}}^2 \tag{13}$$

or

$$\sigma_S^2 = \sum_{i=1}^{n_{pix}} \sigma_{I_i}^2 + n_{pix}^2 \sigma_{\mathcal{B}}^2 + n_{pix}^2 \sigma_{\mathcal{d}}^2 \quad . \tag{14}$$

Since all of the coefficients in Equation 8 are constants, second- and higher-order derivatives in the Taylor expansion are zero and so higher order terms do not appear in Equation 13 and the series converges. Furthermore, over many observations, we expect the variations in the average background, in the digitization offset, and in the signals of individual pixels all to be uncorrelated with one another. Therefore, we have ignored covariance terms in Equation 13.

Now the variance (in electrons, not ADU) in the total signal in each pixel $\sigma_{I_i}^2$ is given by

$$\sigma_{I_i}^2 = \sigma_R^2 + (I_i^* + I_i^D + I_i^S)G \tag{15}$$

where G is the CCD gain in electrons/ADU, σ_R is the read noise, and $I_i^* + I_i^D + I_i^S$ is calculated by subtracting the bias level from the total signal, i.e.,

$$I_i^* + I_i^D + I_i^S = (I_i - I_i^O) \quad . \tag{16}$$

The variance in the average background is given by

$$\sigma_{\mathcal{B}}^2 = \frac{1}{n_B^2} \sum_{j=1}^{n_B} (\sigma_{I_j^D}^2 + \sigma_{I_j^S}^2 + \sigma_{I_j^O}^2 + \sigma_R^2) \quad . \tag{17}$$

Since $\sigma_I^2 = IG$ (photon noise only) and assuming that the bias level is well determined (i.e., $\sigma_{I_j^O}^2 = 0$), we can use the background-equivalent of Equation 16, namely $I_j^D + I_j^S = (I_j - I_j^O)$, to produce

$$\sigma_{\mathcal{B}}^2 = \frac{1}{n_B^2} \sum_{j=1}^{n_B} [(I_j - I_j^O)G] + \frac{n_B \sigma_R^2}{n_B^2} = \frac{1}{n_B^2} \sum_{j=1}^{n_B} [(I_j - I_j^O)G] + \frac{\sigma_R^2}{n_B} \quad . \tag{18}$$

From Equations (11) and (12), we obtain the variance in the digitization offset (in electrons)

$$\sigma_d^2 = G^2 \left(\frac{\sigma_f^2}{n_{pix}} + \frac{\sigma_f^2}{n_B} \right) = \frac{G^2}{n_{pix}} \left(1 + \frac{n_{pix}}{n_B} \right) \sigma_f^2 \quad . \tag{19}$$

We can now substitute Equations 15, 18, and 19 into Equation 14 to obtain

$$
\begin{aligned}
\sigma_S^2 &= \sum_{i=1}^{n_{pix}} \left[\sigma_R^2 + (I_i - I_i^O)G \right] + n_{pix}^2 \left[\frac{1}{n_B^2} \sum_{j=1}^{n_B} \left[(I_j - I_j^O)G \right] + \frac{\sigma_R^2}{n_B} \right] + \frac{n_{pix}^2}{n_{pix}} \left(1 + \frac{n_{pix}}{n_B} \right) G^2 \sigma_f^2 \\
&= n_{pix} \left(1 + \frac{n_{pix}}{n_B} \right) \sigma_R^2 + \sum_{i=1}^{n_{pix}} \left[(I_i - I_i^O)G \right] + \frac{n_{pix}^2}{n_B^2} \sum_{j=1}^{n_B} \left[(I_j - I_j^O)G \right] + n_{pix} \left(1 + \frac{n_{pix}}{n_B} \right) G^2 \sigma_f^2 \quad .
\end{aligned}
\tag{20}
$$

Equation (20) is the final expression for the photometric error in the integration. The first term is the effect of readout noise on both star and background integrations; the second term is the photon noise in the star integration; the third term is the photon noise in the background determination; the fourth term is the contribution from the digitization process. One can see the similarity between the terms resulting from read noise and digitization noise. Because $\sigma_f \simeq 0.289$ for a uniformly distributed f, we can compare the relative magnitudes of these two noise terms by comparing σ_R^2 with $\sim (G/3.5)^2$.

2 H. "CCD EQUATION"

The traditional expression for determining the signal-to-noise ratio of a point-source observation, either after the fact or for planning observations, is the "CCD equation". This equation (*cf.* NOAO/KPNO CCD instrument manuals or Mortara and Fowler 1981; see the Appendix for definitions of parameters) is given by

$$\frac{S}{N} = \frac{N_\star}{\sqrt{N_\star + n_{pix}(N_S + N_D + N_R^2)}} \quad . \tag{21}$$

This expression is naive in the sense that it assumes the background is infinitely well determined and that there is no digitization noise. This is never the case and, as was demonstrated by NEWB91 and repeated below in our own notation, a revised expression for the signal-to-noise ratio yields values that can differ significantly from those given by Equation (21) (especially for "noisy" backgrounds, at low light levels, or at high gain). If we now switch to the conventional notation (*i.e.* that used

in Equation 21) and approximate portions of Equation (20) as follows:

$$\sum_{i=1}^{n_{pix}} [(I_i - I_i^O)G] \simeq N_\star + n_{pix}(N_S + N_D) \tag{22}$$

and
$$\sum_{j=1}^{n_B} [(I_j - I_j^O)G] \simeq n_B(N_S + N_D) \quad , \tag{23}$$

then we can rewrite Equation (20) as

$$\sigma_S^2 \simeq n_{pix}\left(1 + \frac{n_{pix}}{n_B}\right)N_R^2 + [N_\star + n_{pix}(N_S + N_D)] + \frac{n_{pix}^2}{n_B^2}[n_B(N_S + N_D)] + n_{pix}\left(1 + \frac{n_{pix}}{n_B}\right)G^2\sigma_f^2$$

$$\simeq N_\star + n_{pix}\left(1 + \frac{n_{pix}}{n_B}\right)(N_S + N_D + N_R^2 + G^2\sigma_f^2) \quad . \tag{24}$$

Using $N_\star$ as the total integrated signal detected, and σ_S (given by Equation 20) as the correct expression of the noise, we can use Equations 22–24 to write a "revised CCD equation" as

$$\frac{S}{N} \simeq \frac{N_\star}{\sqrt{N_\star + n_{pix}\left(1 + \frac{n_{pix}}{n_B}\right)\left(N_S + N_D + N_R^2 + G^2\sigma_f^2\right)}} \quad . \tag{25}$$

Clearly, the signal-to-noise has a dependence on both the number of star pixels and the number of background pixels used. The larger the number of background pixels selected, the better the correction for background and digitization and the lower the noise. Furthermore, selection of the number of star pixels must be done with care, since arbitrarily large integration areas can degrade signal-to-noise drastically (see Howell 1989). Even more serious, systematic errors can result by choosing the background region too close to the star or in an area that is not representative of the background in the stellar aperture. We stress that Equation (25) is *still* an approximation; the signal-to-noise is better calculated using the more exact error expression given by Equation (20).

We can now make use of the speed of our code and run a series of models with identical input parameters, finding the standard deviation of the batch of integrations produced. In this way we compare this external and independently determined standard deviation with that predicted by the analytical error equations and with that predicted by the traditional CCD equation. These results for three different cases are shown in Figure 1. We plot the cumulative standard deviation: the value plotted for model number n, for example, is the standard deviation (of the background-corrected counts) from the ensemble of successive models 1 through n. The three cases shown in

Figure 1 have identical physical image scales; they differ only in the number of background pixels selected and in the physical pixel size (meaning the number of source pixels integrated is different). As expected, whenever the number of source pixels is large and the number of background pixels is small, the standard deviations are larger and the traditional CCD equation does the poorest job of predicting the signal-to-noise. The error bars on our empirical curve are 95% (2σ) confidence limits. Even after many trials, the empirical standard deviation may be substantially different from the population standard deviation, illustrating the risk in depending too heavily on measured standard deviations based on "small" numbers of observations.

2 I. CURRENT OPTIONS, LIMITATIONS, AND FUTURE DIRECTIONS

Table 1 lists the user-input parameters to our software model, along with a brief definition of each. Also included in this table are the values of these parameters for the various models shown in the figures. The input file itself is nearly identical to Table 1; values may be reviewed and changed quickly and easily. We have tried to make the input parameters as general, yet as easy to understand and use, as possible. Changes are allowed in source, telescope, instrument, and detector characteristics, and the position and size of the integration aperture with respect to the image centroid may be adjusted. In addition, individual noise sources may be turned on or off. The user may request a fixed initial noise seed to reproduce a previous run or may allow the program to select a random initial seed to provide an independent model. The synthetic data are output as simple integrations (one-dimensional), as radial slices (two-dimensional), and as intensity-contour plots (three-dimensional). Each run is tagged with an identification code so relevant input and output data can be logged uniquely.

One limitation that we remedied early in the development, chiefly because of our desire to model (undersampled) Galileo images, was that we were not performing a full two-dimensional integration of the stellar energy profile. This is a drawback, leading to poor photometric results, for many of the widely available reduction packages, whenever the profile is significantly undersampled by the CCD. This problem is discussed further by King (1983), Buonanno and Iannicola (1989) and Holtzman (1990). We have now successfully incorporated this into the model.

There are a number of limiations to the current model. Perhaps the most important is that we have not yet investigated the effect of fixed-pattern noise on accurate photometry of point-sources.

The magnitude of this noise is proportional to the signal level and therefore is significant when the exposure is a substantial fraction of full-well. It also depends on the degree of the pixel-to-pixel differences in quantum efficiency. Our original design for this model was for low-light-level, low S/N applications. Therefore, this version of the model makes the pixel sensitivities uniform and constant, using the same fixed quantum efficiency for each pixel. Certainly, one can derive expressions for the errors involved in flat-field corrections, as did NEWB91, but creating a realistic model of flat-field variations and corrections is more difficult. This is because the variations usually cannot be, and are not routinely, characterized by one or a few simple parameters, as is read noise. Future revisions will include fixed-pattern noise.

We did not integrate fractional pixels in the initial version of the program. The reason is not that it is difficult, but rather that it may be misleading. In practice, using a real detector, fractional pixel integration would require assumptions about the the PSF and the image center. Using the model's input PSF and center would make the computation circular, giving back what we put in, plus noise. We did not want, at this stage, to attempt to fit the output of the program with another PSF or attempt to find centers; that is best left to the user's own reduction programs. As a consequence, photometric output values will be somewhat sensitive to the selected r; in fact, many of our tests have involved study of this sensitivity. Our main goal is the production of a reliable CCD image (not accurate photometry), which can then be integrated in any way one chooses. We will to add fractional pixel integration of the model output as an option.

The present version of the model also does not treat the stellar flux, the earth's atmospheric transmission, the transmission of the filter, or the detector quantum efficiency as functions of wavelength (see Equations 1 and 2). While it should work well to get a general idea of the photometric accuracy expected for a given situation, detailed comparisons of various detectors on specific stars may be somewhat uncertain. The shape of the point-source profile itself may not be quite correct for all images at all observatories. If telescope aberrations are not large, we do not expect this limitation to be a problem. We do not yet allow for non-circular integration windows, rectangular (non-square) pixels, or inter-pixel gaps. Changes in system characteristics such as readout noise that may accompany such functions as pixel-binning have not been implemented. Furthermore, we presently assume that there is no error in determination of the read noise and bias level, which is unrealistic.

Many of the systematic errors, such as overestimating the background or problems with chip defects, are difficult to estimate except in specific cases and will not be added as a routine mechanism in the noise model. In addition, detector or A/D effects that are difficult to parameterize have not been added at this point. We also do not address other problems, such as fringing, scattered light, diffraction spikes, radiation events, and charge transfer efficiency. This model is intended to model a single star on the detector, so variations of the PSF and background over the CCD would have to be determined by the user beforehand. Jacoby, Ciardullo, and Ford (1990) discuss correcting for variable background over the CCD.

Work is in progress on many of the areas above to improve the code. We hope to expand this work to begin modeling extended sources such as galaxies, planets, comets, and asteroids. The effect of changes in reduction procedures involved in background subtraction or flat-fielding, for example, will also be examined in detail. We hope to be able to add simulations of the many problems found in real CCD systems once we determine how best to parameterize them, such as flat-field, A/D differential linearity, and variation of PSF and background over the detector.

3. INITIAL RESULTS

In this section, we present models calculated using the above prescription. For the most part, they are based on the parameters associated with current or previous Kitt Peak CCD/telescope combinations as described in the NOAO/KPNO instrument manuals. This was done not because of limitations in our model, but because we wanted to use a consistent set of data. Table 1, which gives the user-input parameters to our program, also includes listings of the parameters used in the models discussed in this section.

The parameter space from which we choose our example models is quite large. We present here only a few examples, which we hope are illustrative. The first part of this section discusses two models calculated for $V = $ 16th and 20th magnitude point-sources. These will be examined in some detail to show the possible uses that can be made of the output "data" as well as to present information gained from a comparative study. We will then look at various other models that are included to demonstrate the range over which our program can function and to elucidate interesting and possibly previously unknown properties associated with point-sources imaged on CCDs.

In our discussion below we will use the terms "bright" and "faint" as descriptions for specific point-source models. As a working definition we use the following: a "bright" source is one for which the observation yields adequate S/N out to a radius r, which is the radius at which the PSF becomes independent of seeing effects. Thus, the terms bright and faint are not quantitative but relative terms (see Howell 1993). Their use requires a good understanding of the signal and noise sources involved.

We use the Axum^{TM} graphics package (TriMetrix, Inc.) on a PC to make all the plots. The 3-D plots are made as pixel histograms rather than the common spline surface fits. We use the histograms because spline fits tend to smooth out the real features in a 3-D plot, masking the true, detailed nature of the image.

3 A. 16th AND 20th MAGNITUDE MODELS

Figure 2 shows the two models discussed in this section; both simulate a Texas Instruments (TI) CCD. Notice that the brighter source could be approximated nicely with a Gaussian function while the 20th magnitude object is highly asymmetric and merges with the background in a complex and unknowable manner.

Figure 3 shows the same models but displays separately the contributions of each individual component of the raw count. The raw count is that presented to the CCD user directly after readout. In the signal from a given image, the original source of any individual electron cannot be determined. That is, whether a particular electron was the result of a dark event, a stellar photon, a sky photon, or the electronics, only their sum in each pixel is known. The curve labeled "BG corrected counts" shows what remains after the mean background level (sky + bias + dark) is subtracted. The level of each source of counts is shown independently in the remaining three curves of each figure. Note that for the 20th magnitude star, the raw and bias counts have had 500 ADU subtracted to show detail in each of the curves.

One often faces the problem of knowing where the star's flux distribution effectively ends and the "pure" background begins, *i.e.* the problem of choosing the physical integration limits. We can see from Figures 2 and 3 that this problem gets increasingly worse as the S/N of the observation decreases. Obviously there is not an exact cutoff but rather a transition region. For a brighter star this transition usually can be determined easily and often is relatively unimportant, for example,

in terms of performing aperture photometry. For fainter stars, however, the radius at which the
pure background begins is not clear at all.

A solution to the difficulties associated with knowing exactly where the point-source "ends"
and the background "begins" is to use growth curves. The method of using CCD growth curves
for obtaining more accurate aperture photometry, especially for low S/N observations, had been
discussed somewhat (Da Costa, Ortolani, and Mould 1982), but recently is getting more attention
(Howell 1989, Stetson 1990a, Howell 1992). Adding the 2-D flux within each of several successive
radii from the point-source, one produces data like those shown in Figure 4. Each point in these
plots is based on the average of four independent model calculations. This was done in order
to simulate the construction of these curves from more than one source on a given CCD frame
(*cf.* Stetson 1990a,b). The error bars are the calculated standard deviations of an integration
(see Equation 20) within that particular radius. At large radii, a great number of noisy pixels are
encountered (see Howell 1989) and, as predicted by the noise equations, the error increases.

These curves are exactly what one expects to get from real data and several methods of
calculating and presenting CCD growth curves have been discussed in the literature; for example,
see Howell (1989, 1990a,b) and Stetson (1990a,b). Howell (1989) also discussed the S/N ratio as
a function of radius from the star and showed that 1) for a given point-source, there is a specific
radius at which the S/N is the greatest and 2) that this radius *is not* the same for each source,
even on a given CCD frame.

Figure 5 indicates how much of the total signal is captured as a function of radius of the
integration aperture for our PSF. Thus, one might be lead to believe (and, indeed, as was done by
necessity for years with photoelectric photometry) that one must use an aperture of ~3 FWHM to
capture essentially "all" of the starlight. While that statement is true, the optimum aperture size
to use for CCD photometry is usually considerably smaller.

In Figure 6 both the standard S/N, calculated from the "CCD equation" (Equation 21),
and the S/N calculated from the revised CCD equation (Equation 25) are shown. We see that
the standard equation consistently overestimates the S/N obtainable, although at the optimum
aperture, the two methods do not predict substantially different S/N. In general, the (percentage)
difference between the S/N predicted by the two methods becomes increasingly greater as the
source gets fainter.

Two observations may be made here. One is that, if one were to use the "traditional"-size aperture of about 3 FWHM, then use of the CCD equation would predict a considerably higher S/N than this model would, and hence, the observer would underestimate the amount of telescope time needed for a project, perhaps misjudging whether the project could be done at all. The second is that the CCD equation, at least for brighter stars, would predict an "optimum aperture" that would ultimately lead to lower S/N than is possible, as can be seen from Figure 6. Thus, our model can be used to accurately explore detector and observational parameters before data are taken, ensuring quality observations.

3 B. BACKGROUND PIXELS

We have seen that the standard CCD equation overestimates the quality of a measurement and that a more accurate equation for the S/N of a point-source is given by Equation (25). This equation has a dependence on the number of pixels used to determine the background. We now explore this dependence for two sky conditions using a TI CCD with 2×2 pixel binning and a bright point-source. The results of this simulation are shown in Figure 7. The CCD equation again gives a consistently higher value than the model and shows little dependence on the number of pixels used for background determination. This lack of sensitivity to the choice of background is expected from the form of Equation (21). It is apparent here because of the high flux of the source and hence a relatively low noise in the background. If one would repeat this figure for a fainter source, the S/N predicted by the CCD equation would be more erratic but would approach a single value as the number of background pixels increased. This is not because there is any explicit dependence on the number of pixels used, but because as the number increases, the S/N calculated would reflect the statistically better estimate of the true background.

As expected, the S/N calculated by the model shows a strong change with the number of pixels used. It correctly predicts that a series of integrations will have lower than optimum precision whenever the background is poorly sampled and its "correct" value is not well known. As the number of background pixels increases, our model S/N approaches its limiting value. This value is reached in this case, and for all other models we have run, when the number of background pixels used is about three times that used in the source aperture.

Use of a model such as this allows one to test this value at will. In the case shown here, the number of pixels used in the source aperture is 69. We see that the number of background pixels needed for a statistically significant sample is approximately 210. This behavior can be predicted directly from Equation (25) since $S/N \propto (1 + \frac{n_{pix}}{n_B})^{-\frac{1}{2}}$. In real cases however, there are some limitations on the number pixels that can be used for background determination. Factors such as the degree of crowding of the imaged field or the uniformity of the background over the frame, can sometimes make the choice of the number of background pixels inflexible. For these situations, however, we would at least like to derive the best possible statistical errors.

3 C. IMAGE PLACEMENT ON PIXEL GRID

The models so far have always placed the point-source exactly at the center of a pixel. Of course, this situation would be fortuitous in reality. We have therefore calculated a model (Figure 8) using the 4-m telescope and a Tektronics (TEK) CCD that was first centered within pixel $(50, 50)$, and then offset in y only, then in both x and y. The profile changes are quite apparent and one can imagine that they are even more dramatic for fainter sources or extended sources, where the shape of the object and the light distribution is not known *a priori*. In other tests, such as those we are performing in modeling Galileo images, the effects of image placement is even more dramatic because of the narrow profiles with respect to the pixel size. Such visualization can provide insight when designing computer techniques for data reduction and analysis because not all profiles will look like 2-D Gaussians centered at the apparent centroid of flux.

3 D. FAINT BACKGROUND OBJECTS

When performing photometry from a CCD frame, two of the big advantages over the traditional use of a photomultiplier tube, with its single collecting aperture, are that centering can be done after the fact and that the 2-D imaging allows optimally-sized software apertures to be defined on a frame-by-frame basis if needed. In addition, the user can identify and eliminate close companions or background sources, and the background counts (and noise) per sampling element are reduced (one pixel vs. entire photocathode). These problems are difficult to address with a PMT-type single aperture. We have seen above that the centroid of a faint source is not necessarily easy to

determine; it requires care and thought, at least in some cases. We now address another supposed advantage, that of being able to identify and eliminate close companion sources.

During the time interval necessary to take a series of frames (say for time series work or to obtain multiple colors) or even during a single frame, the seeing and position of all objects imaged will change slightly. There are other effects that are time variable as well, such as focus or guiding errors, but we limit this discussion for simplicity. Figure 9 shows four models of a faint object observed under two different seeing conditions and two grid positions, using a Tektronics CCD on the 4-m telescope with a 1200 second exposure. Figure 10 shows radial profiles for the four cases shown in Figure 9. The S/N of each observation is low and the chance for recognition of the object by visual or software inspection varies depending on the frame. In fact, we notice that the combination of poor seeing, pixel registration, and the statistical nature of the various noise sources even causes the centered image (Figures 9c, 10) to be "lost" in the background while in Figures 9d and 10, the non-centered source may be discernable. Sources of this type no doubt abound in many CCD frames and can cause effects such as erroneous magnitude determinations or artificial 2-D image structure. To be sure, this type of error is generally small and for most cases can be ignored. We draw attention to this analysis simply as a reminder that even with CCDs, reductions can be difficult. When living in the realm of low S/N observations, care must be exercised and use of modeling techniques can show the user where such problems may arise (Howell 1992, 1993).

3 E. USING DIFFERENT CCDs

Our last sample model is shown in Figures 11 and 12. The point-source and integration time are the same in all cases. The images appear different because of the differences in the CCD properties such as detector gain and image scale (a combination of pixel size and telescope magnification). It is clear that images of the same source taken over time, but with different CCDs, may look very different. One must be aware of this possibility, especially when trying to extract 2-D structural information from an image. Our software model can quickly give users insight into how changes in specific instrument characteristics will affect the 2-D structure in their images. These models are included here to illustrate once again that a CCD user must be somewhat knowledgeable about specific chips and aware of how the data will appear on the CCD being used. Keep in mind, some CCDs may be more suited than others for a particular observational program.

Table 1
INPUT PARAMETERS FOR SOFTWARE MODEL
(WITH VALUES USED IN FIGURES)

USER-INPUT PARAMETERS (units)		MODEL PARAMETERS FOR EACH LISTED FIGURE						
		1a,b,c	†	7	8a,b,c	9a,b 10	9c,d 10	11a,b,c 12
SOURCE CHARACTERISTICS								
SPTYPE	spectral type (CHARACTER)	A0	A0	A0	A0	A0	A0	A0
VMAG	V magnitude of object (mag)	17.0	16.0,20.0	17.0	19.0	24.0	24.0	18.0
ENVIRONMENTAL CHARACTERISTICS								
SKYMAG	sky brightness (mag/arcsec²)	21.5	21.6	19.0,22.0	19.0	19.0	19.0	20.0
FWHM	FWHM of seeing disk (arcsec)	2.0	1.5	1.6	1.0	1.5	3.0	1.4
ZENITH	zenith angle of source (degree)	0.0	0.0	0.0	0.0	0.0	0.0	0.0
TELESCOPE/INSTRUMENT/FILTER CHARACTERISTICS								
DIAMTEL	diameter of telescope primary (m)	0.91	0.91	0.91	3.76	3.76	3.76	0.91
DIAMSEC	diameter of secondary obstruction (m)	0.43	0.43	0.43	1.54	1.54	1.54	0.43
EFFIC	efficiency of entire optical path (%)	49	49	50	50	50	50	50
IMGSCALE	image scale (arcsec/pixel) [=(arcsec/pixel)*1000/PIXSIZE]	30.00	28.67	27.67	20.00	20.00	20.00	27.67,67,67,28.52
LAMBDA0	central wavelength of bandpass (Å)	4400	4400	4420	6470	6470	6470	5465
BANDPASS	effective width of bandpass (Å)	980	980	1110	1110	1110	1110	1130
arcsec/pixel ‡		0.45,0.45,1.05	0.43	0.83	0.54	0.54	0.54	0.42,0.83,0.77
DETECTOR CHARACTERISTICS								
QE	mean quantum efficiency over BANDPASS (%)	45	45	60	35	35	35	65,72,40
PIXSIZE	pixel size (microns)	15,15,35	15	30	27	27	27	15,30,27
RN	CCD read noise (e/pixel/read)	30.0	8.0	8.0	30.0	30.0	30.0	8.0,75.0,7.8
GAIN	CCD gain (e/ADU)	15.0	4.15	4.00	10.00	10.00	10.00	4.00,11.00,3.20
BIAS	CCD bias level (ADU)	500	550	550	550	550	550	550
INTEGRATION-DEPENDENT CHARACTERISTICS								
X0	centroid of point-source in x (pixels)	50	50	50	50,50,50.72	50,49.5	50,49.5	50
Y0	centroid of point source in y (pixels)	50	50	50	50,50.37,50.37	50,50.4	50,50.4	50
XA0	aperture center for model integration in x (pixels)	50	50	50	50	50	50	50
YA0	aperture center for model integration in y (pixels)	50	50	50	50	50	50	50
RANGE	radius of model integration (units of FWHM)	2.5	0-3.5	2.5	3.0	3.0	3.0	2.5
LIMRX1	x start for radial slice (INTEGER pixel)	50	50	50	50	50	50	50
LIMRX2	x end for radial slice (INTEGER pixel)	60	80	70	70	70	70	70
TIME	exposure time (seconds)	300	120	120	30	1200	1200	180
NOISE-SOURCE OPTIONS								
NBKGD	# of pixels in background (INTEGER pixels)	100,400,100	200	10-500	200	200	200	200
ISEED	Initial seed for noise (random = 1, same = 0)	1	1	1	1	1	1	1
NOISEB	sky noise (on = 1, off = 0)	1	1	1	1	1	1	1
NOISES	source noise (on = 1, off = 0)	1	1	1	1	1	1	1
NOISER	read noise (on = 1, off = 0)	1	1	1	1	1	1	1
NOISED	digitize data (yes = 1, no = 0)	1	1	1	1	1	1	1

† This column is for parts a, b of Figures 2, 3, 4, 6.   ‡ Derived quantity; Not an input parameter.
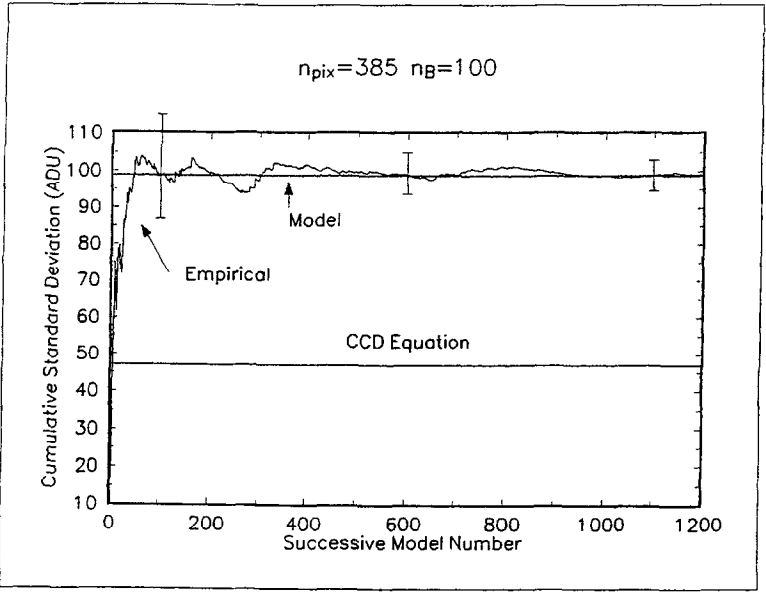
Figure 1a (Merline and Howell)

Figure 1b (Merline and Howell)

$n_{pix}=69$ $n_B=100$
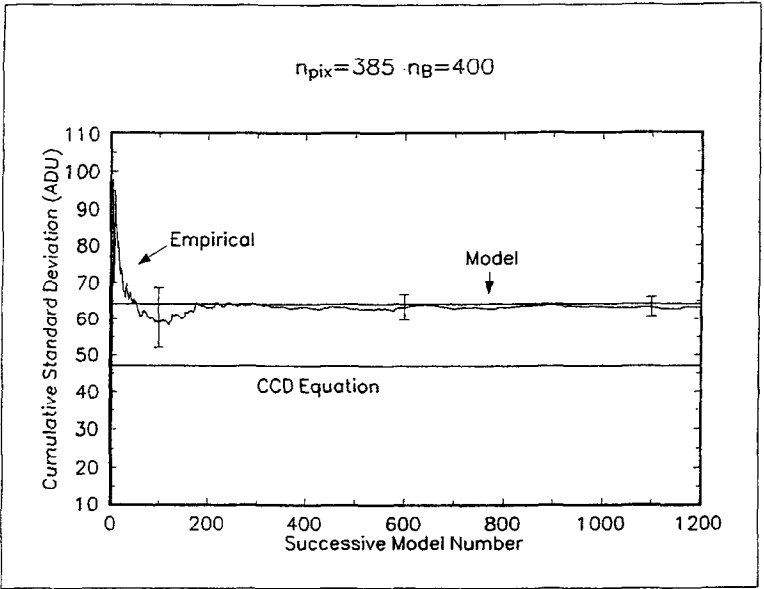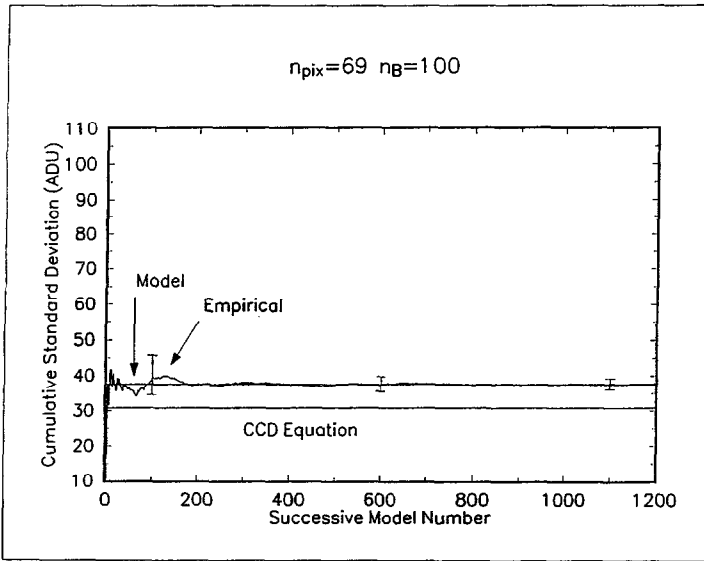
Figure 1c (Merline and Howell)

Fig. 1 — Multiple runs using the same input characteristics can be used to test the validity of our analytical error expression. Each plot shows the cumulative standard deviation of the integration values in a series of point-source models (empirical curves). Three cases (a,b,c) are shown. Within each case, the models all use the same values for input parameters and differ only in the random variations. By cumulative, we mean that the value plotted for successive model number n is the standard deviation of the sample of models 1 through n. Thus, with enough trials one should eventually reach a good estimate of the true (or population) standard deviation. We have also plotted the predicted standard deviation based on both our newly derived expression (Equation 20) and the traditional CCD equation. The plotted error bars represent 95% confidence limits. The three cases shown here have identical physical image scales, but differ in the number of background pixels, n_B, used and in the physical sizes of the pixels (and so differ in the number of source pixels, n_{pix}, integrated). Since the signal is the same for all three models, the S/N is being determined by the pixel size and number of background pixels. For these cases, our model clearly does a better job of predicting the error to be expected than does the CCD equation. Note the large uncertainty of the measured standard deviation, even after many trials. Table 1 gives a complete list of the software input parameters for all the figures.
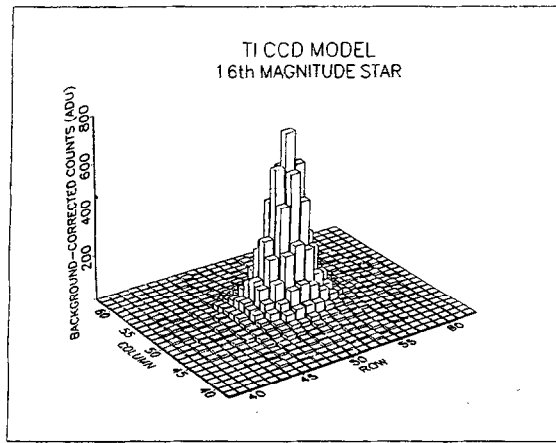
Figure 2a (Merline and Howell)
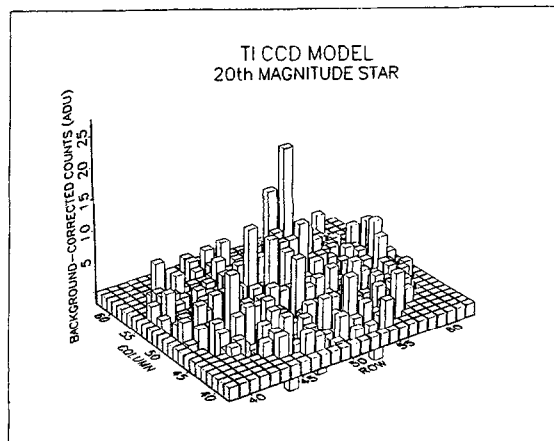
Figure 2b (Merline and Howell)

Fig. 2 — Models for stars of (a) 16th and (b) 20th magnitude (120s exposure on 0.91 m telescope). The plots show the *background-corrected* intensity distribution of the point-source as imaged on the CCD. As the source gets fainter, the distinction between source counts and background counts becomes less clear. Note that the intensity distributions of the 16th magnitude star probably could be well-represented by a Gaussian function, while that of the 20th magnitude star could not. The models are calculated only out to a given radius; therefore, in the 3-D figures, all pixels beyond this range will have zero counts.
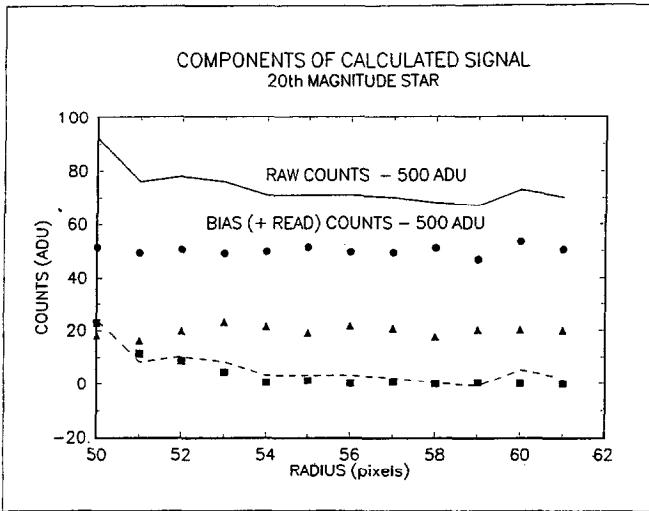
Figure 3b (Merline and Howell)
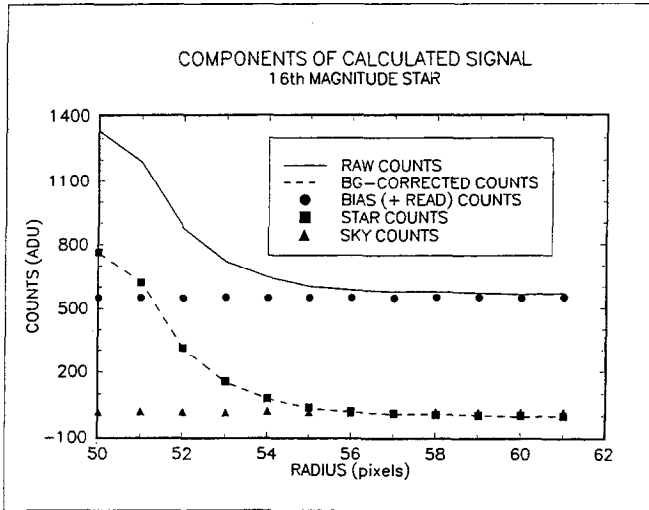
Figure 3a (Merline and Howell)

Fig. 3 — Radial profiles corresponding to the point-sources of Fig. 2. The five curves in each plot show each signal source separately, as well as the raw and background-corrected counts. Background-corrected counts are those that remain after subtraction of dark, sky, and bias. Note that the 20th magnitude source is not well differentiated from the background.
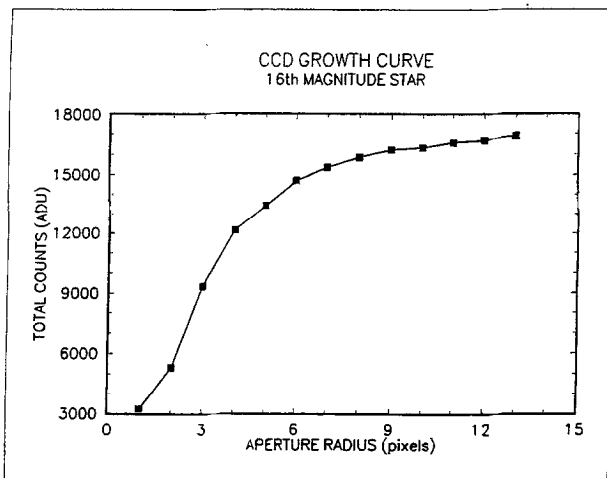
Figure 4a (Merline and Howell)
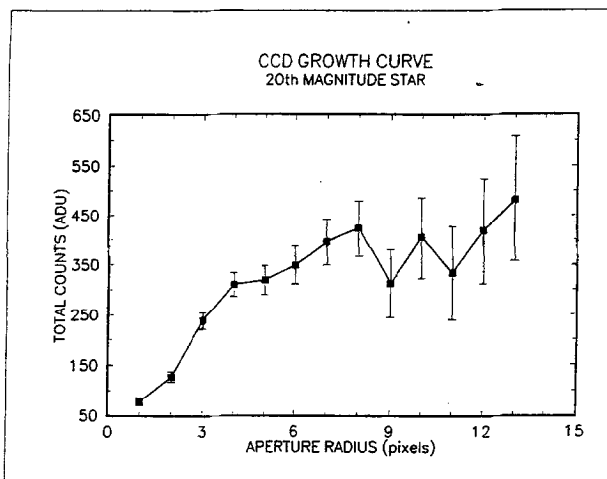
Figure 4b (Merline and Howell)

Fig. 4 — CCD growth curves for the models in Fig. 2. Growth curves are created by summing the total counts within circular apertures of ever increasing radius, centered at the flux centroid. They can be of great use for determining accurate photometric values of point-sources with particular application to crowded fields and faint (low S/N) sources. The curves were constructed using average values from four runs of each model. The error bars are from Equation 20; those for the 16th mag models are smaller than the size of the symbols.

TOTAL SIGNAL vs. RADIUS
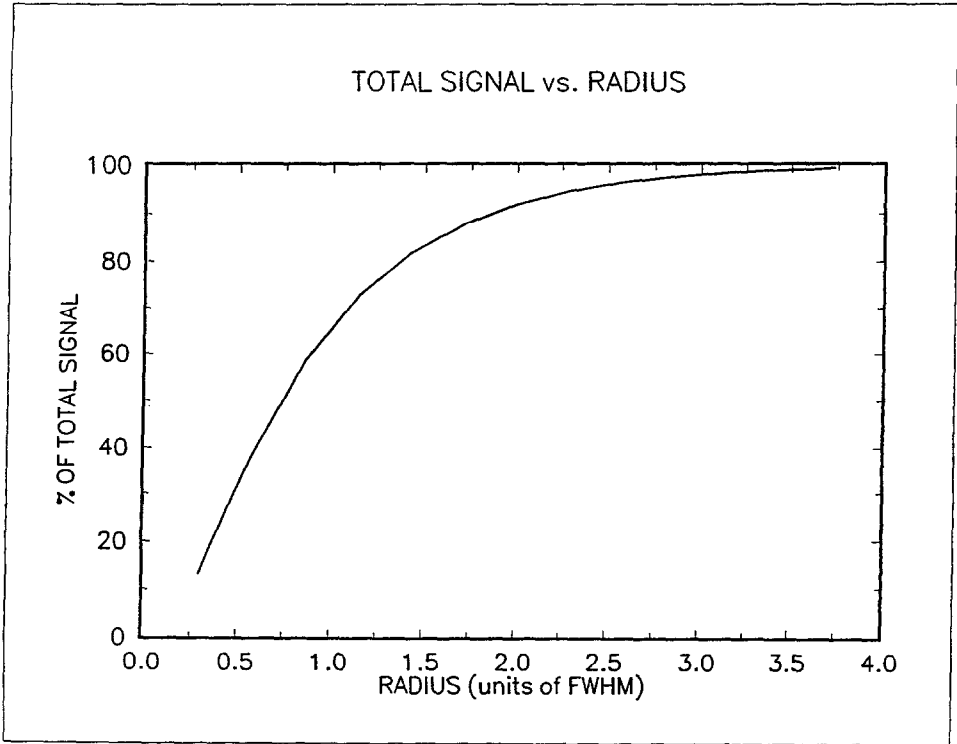
Figure 5 (Merline and Howell)

Fig. 5 — Curve showing the amount of total signal contained within a given radius for our (typical) stellar point spread function (see Equation 5). A circular area of radius 3.0 FWHM contains ~98% of the total flux.
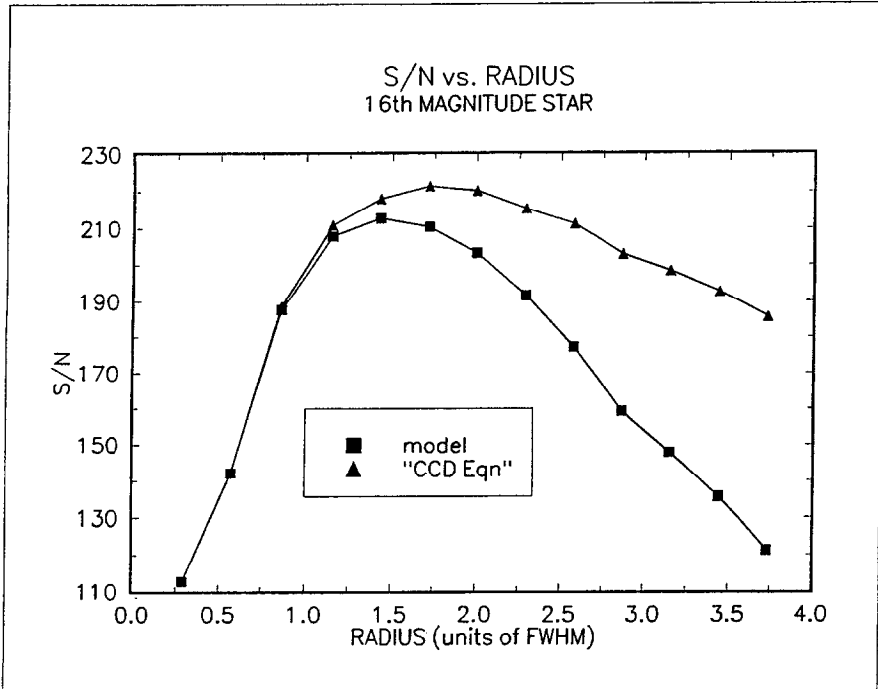
Fig. 6 — The signal-to-noise curves for the two models shown in Fig. 2. They show the S/N predicted by the traditional CCD equation (Equation 21), which consistently overestimates the true S/N for a given point-source, and that predicted by the revised equation (Equation 25). The separation between these two predictions grows as the radius of the aperture increases. In addition, the difference will generally be less for brighter sources because of the diminished importance of the background noise. At a radius of 3.0 FWHM for the examples shown, this difference is 25% for the 16th mag model and 49% for the 20th mag model. In addition, the choice of "optimum" aperture size would be different with each of the two methods.

S/N vs. RADIUS
20th MAGNITUDE STAR
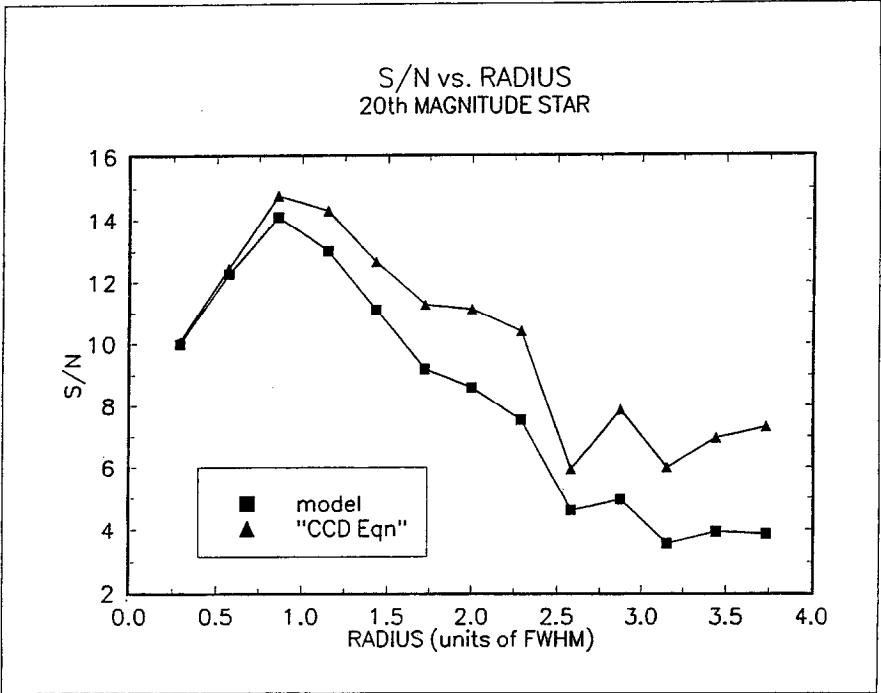
Figure 6b (Merline and Howell)

S/N vs. NUMBER OF BACKGROUND PIXELS
BRIGHT and DARK SKY

<div align="center">
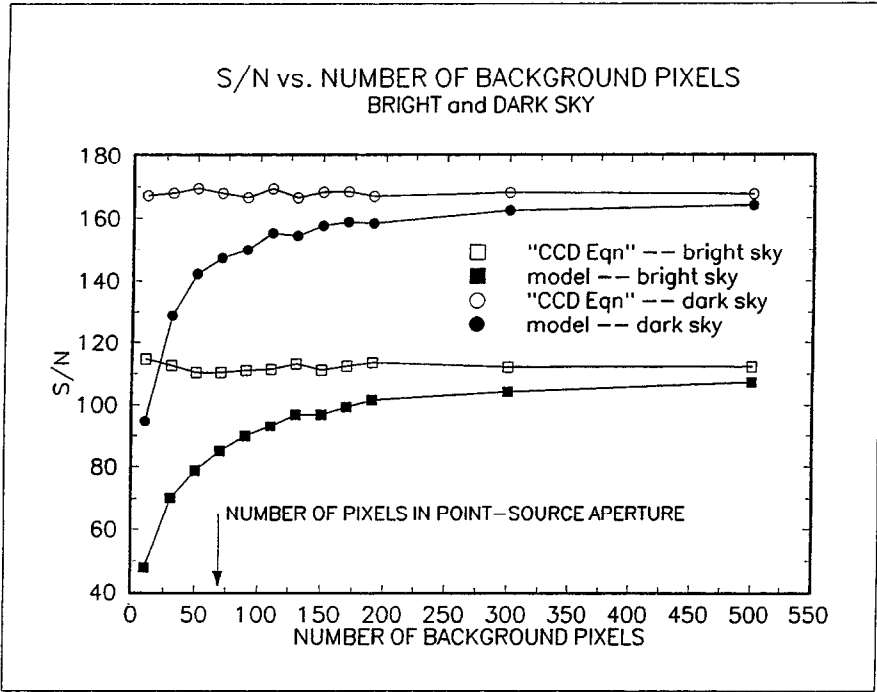
Figure 7 (Merline and Howell)

</div>

Fig. 7 — This figure shows how our S/N estimator compares with the traditional "CCD equation", for two different background (sky) conditions, as a function of the number of pixels used to determine this background level. All observations are of relatively bright point-sources; dark and bright sky refer to new- and full-moon conditions. As the number of pixels used in the background determination increases, the two equations approach limiting and more nearly equal values. The traditional CCD equation has essentially no dependence on the number of background pixels used and therefore always predicts about the same (overestimated) value of the S/N. The number of pixels used within the point-source aperture is shown by the arrow and when $\sim$3 times that number of pixels are used to determine the background, the S/N is adequately determined (see Section 3B).
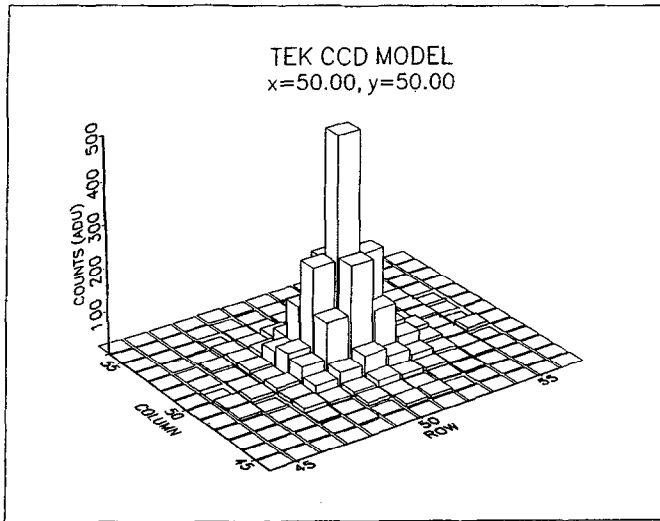
Figure 8a (Merline and Howell)
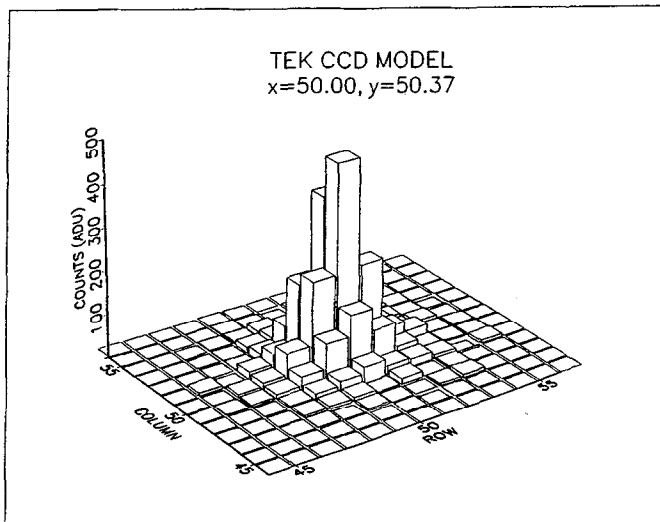
Figure 8b (Merline and Howell)

Fig. 8 — Three models of the same point-source imaged onto a TEK CCD. These models show the varying aspect that the same object can present to an observer, and to the software used for analysis, simply by a change in the physical registration of the image with respect to the pixel boundaries. The listed values of x, y are for the centroid of the modeled point-source.
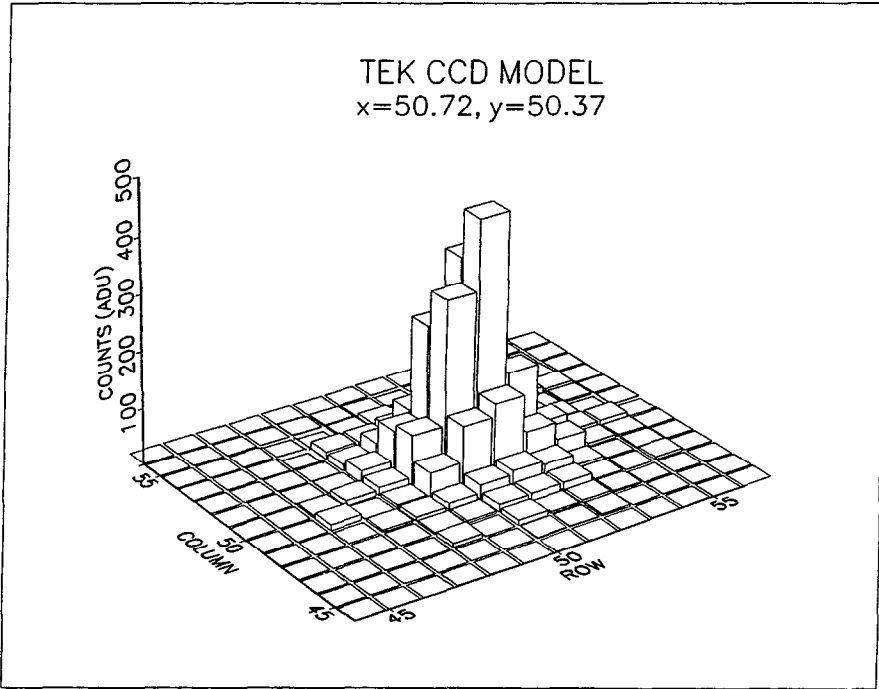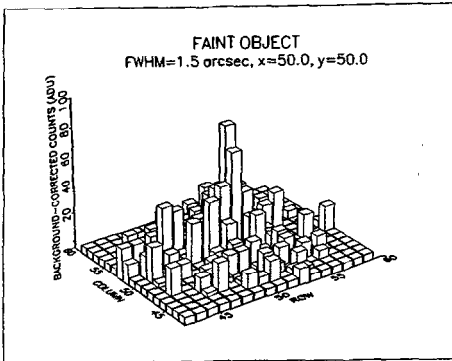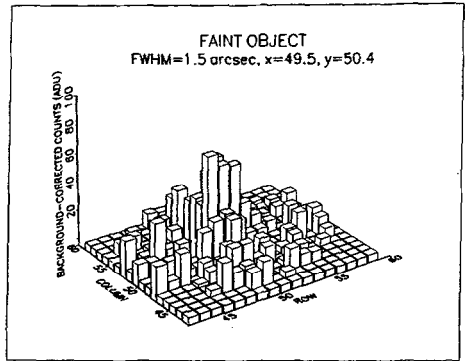
Figure 8c (Merline and Howell)
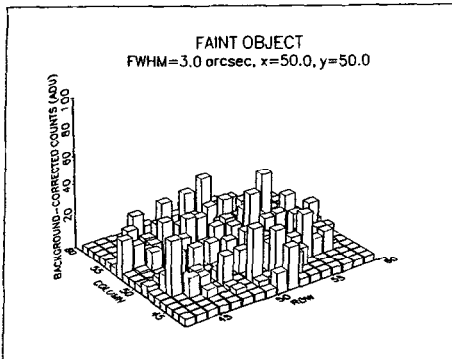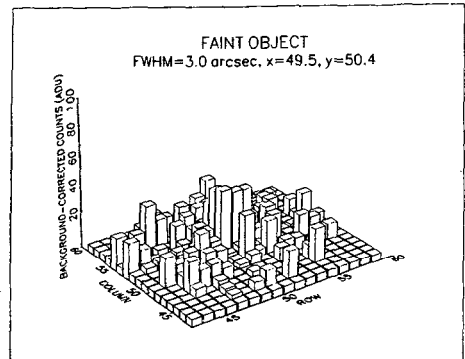
Fig. 9 — Four models showing the same faint object falling slightly differently on the pixel grid, under two different seeing conditions. These models simulate a faint background star or galaxy that will "come and go" throughout a given frame or a series of frames. Since detecting it may be difficult, it could have an effect on background determination or source-flux determination, depending on where the faint object falls with respect to the source of interest.
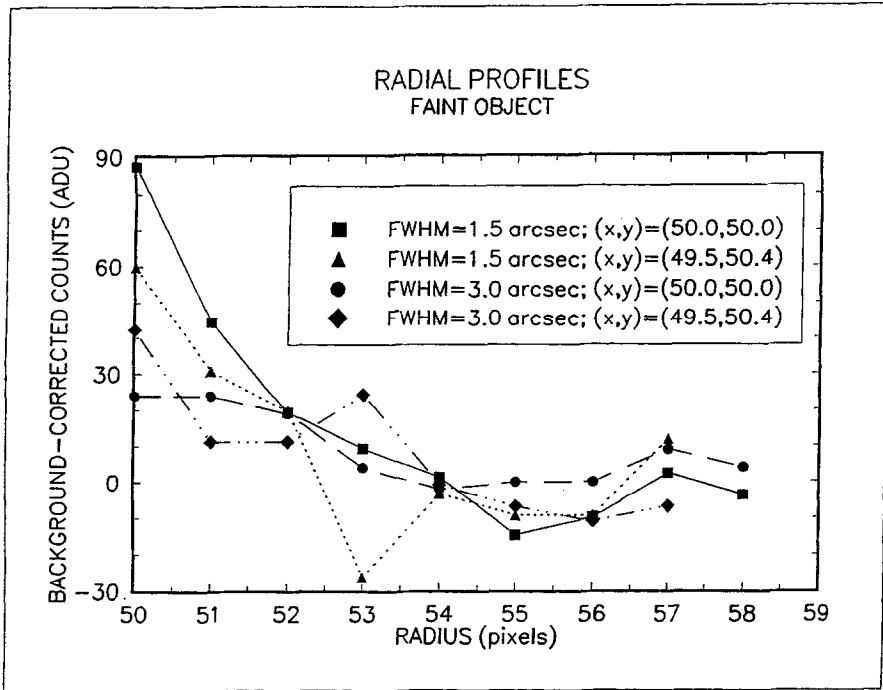
RADIAL PROFILES
FAINT OBJECT

■ FWHM=1.5 arcsec; (x,y)=(50.0,50.0)
▲ FWHM=1.5 arcsec; (x,y)=(49.5,50.4)
● FWHM=3.0 arcsec; (x,y)=(50.0,50.0)
◆ FWHM=3.0 arcsec; (x,y)=(49.5,50.4)

RADIUS (pixels)

BACKGROUND–CORRECTED COUNTS (ADU)

Figure 10 (Merline and Howell)

Fig. 10 — Radial profiles for the four cases shown in Fig. 9.
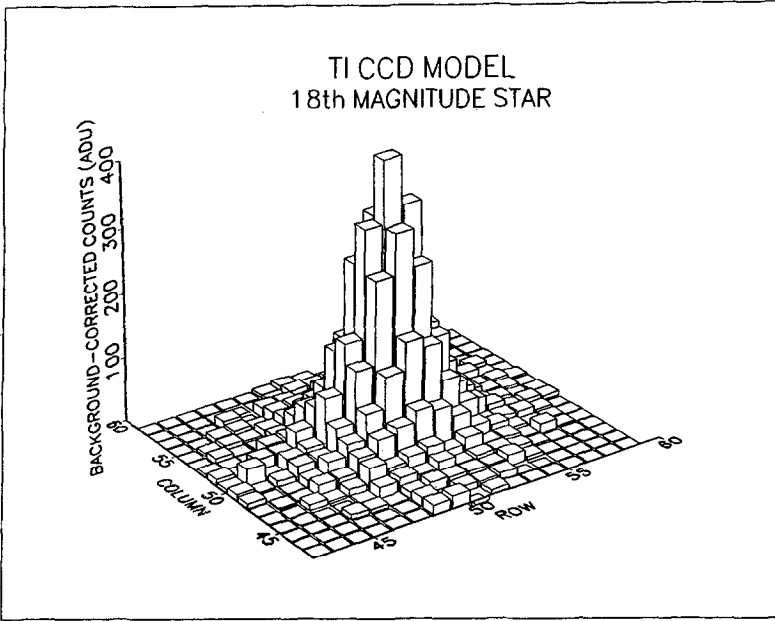
Figure 11c (Merline and Howell)
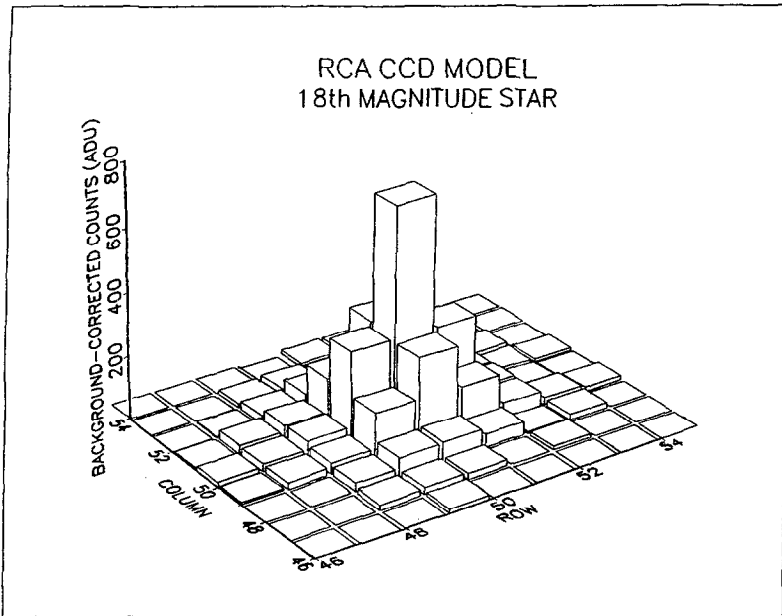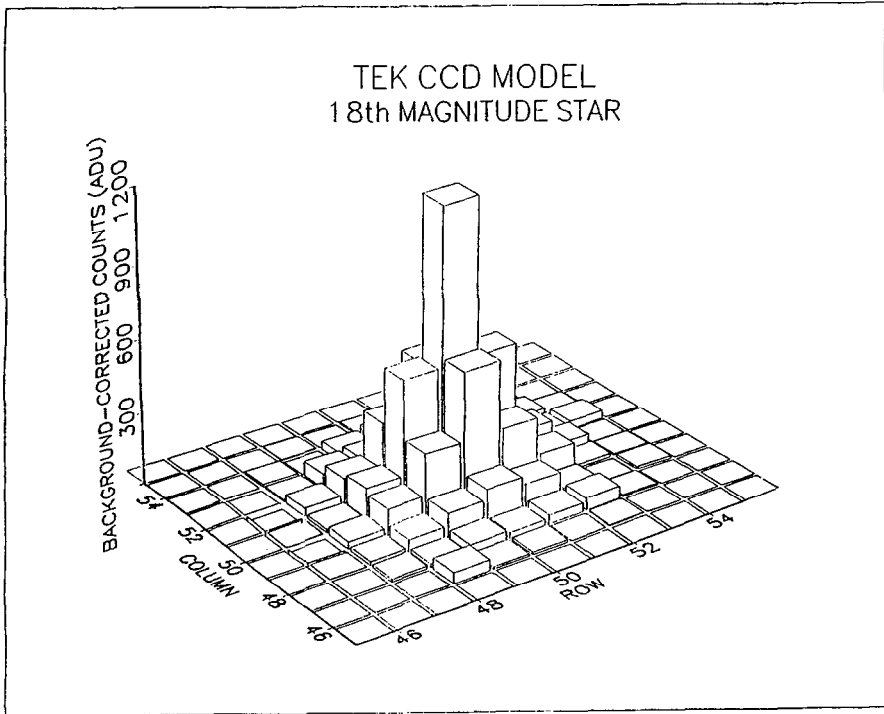
Fig. 11 — An 18th magnitude point-source (180s exposure on 0.91 m telescope) is shown here imaged three times in exactly the same way, except that in each case a different CCD is used. TI, RCA, and TEK CCDs have been modeled to demonstrate the apparent changes in profile, count in the peak pixel, etc. that occur. The changes are simply due to the specific characteristics of the CCD system, such as pixel size and gain. Such changes may be of concern to those interested in the 2-D structure of images, say of extended sources, when observations are made with different CCDs.
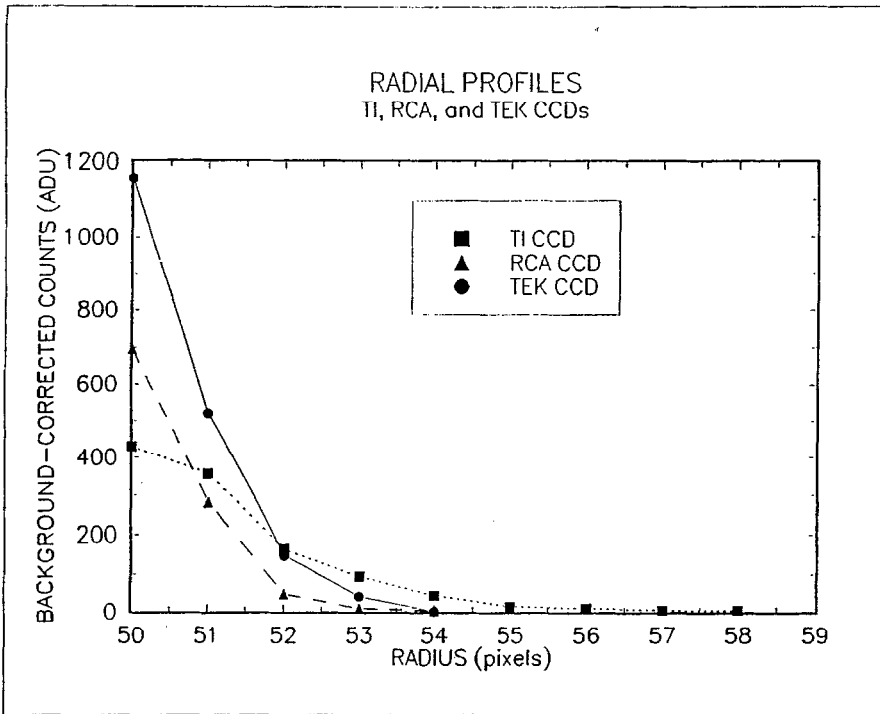
Figure 12 (Merline and Howell)

Fig. 12 — Radial profiles for the three models shown in Fig. 11.

4. SUMMARY

We have developed a flexible computer model for imaging of point-sources with CCDs which is easy to use, but also realistic. Although lacking in a few details, the model can be used to provide improved estimates for the signal-to-noise obtainable under a given set of conditions either before or after actual observations are made, including such effects as systematic errors caused by digitization, which does not appear in theoretical expressions for CCD noise.

Use of our software model has allowed us to confirm and quantify three points. First, that the use of traditional (say $r \sim 3\,\mathrm{FWHM}$) apertures for photometry of faint point-sources can lead to degradation of the overall S/N because of the large contribution to the noise compared with signal from the large number of pixels near the periphery of the aperture. That is, the number of pixels in the source aperture is important. Second, that the number of pixels used to estimate the background is also important and must be considered when planning observations and estimating errors. This is because the process of background subtraction is noisy (because of statistical fluctuations in the sky counts, read noise, and digitization noise) and improves with increasing numbers of background pixels. Third, that the improved CCD equation leads to more realistic estimates of errors for point-source photometry.

We are currently making use of this model to explore better reduction techniques, especially for real-time reduction and analysis of time series data. This is likely to include applications to differential photometry and detailed modeling of growth curves, particularly for faint and partially crowded sources.

We have made extensive use of this code for modeling spacecraft detector systems, including NEAR/MSI and especially the Galileo SSI. We have also used the code in planning for and analysis of both ground-based and Galileo observation of the impact of comet Shoemaker-Levy 9 with Jupiter (see Howell and Merline 1995), and for simulations of a ground-based, photometric search for other planetary systems using data from the Lowell Observatory Near-Earth Object Survey (LONEOS) (see Howell 1995). We have used the model to predict exposure times, signal levels, noise components, and errors for a number of potential ground-based observing runs. It has also been used to aid the process of selecting detectors for use in a program to monitor sky brightness for the National Park Service.

We are making a number of improvements to our model with the intention of making it completely general. In the near future, we hope to extend the versatility of the current software to model images of 2-D or moving sources, such as galaxies or asteroids.

The code is written entirely in FORTRAN and is intended for use as a stand-alone program on a PC/AT-class machine with a floating point coprocessor and the standard compliment (640 kbyte) of memory, although it can be and has been adapted to other machines, such as a Sun SPARC platform. We are using *Microsoft* ⑧FORTRAN Version 5.0. The source code for the program and the associated subroutines require about 42 kbytes; the size of the executable file is 69 kbytes. On a 20 MHz *Dell*^{TM} System 220 PC/AT, a model can be produced in under 30 seconds.

ACKNOWLEDGMENTS

REFERENCES

Adams, M., Christian, C., Mould, J., Stryker, L., and Tody, D. 1980, *Stellar Magnitudes from Digital Pictures* (Tucson, AZ: Kitt Peak National Observatory).

Allen, C. W. 1973, *Astrophysical Quantities,* Third Edition (London: Athlone).

Bevington, P. R. 1969, *Data Reduction and Error Analysis for the Physical Sciences* (New York: McGraw-Hill).

Bottaccini, M. R. 1975, *Instruments and Measurement* (Columbus, OH: Charles E. Merrill Publishing Co.).

Buonanno, R., and Iannicola, G. 1989, *Pub. A. S. P.*, **101**, 294.

Da Costa, G. S., Ortolani, S., and Mould, J. 1982, *Ap. J.*, **257**, 633.

Diego, F. 1985, *Pub. A. S. P.*, **97**, 1209.

Djorgovski, S. 1984, in *Proc. of the Workshop on Improvements to Photometry,* ed. W. J. Borucki and A. Young, NASA Conference Pub. 2350, p. 152.

Gilliland, R. L., and Brown, T. M. 1988, *Pub. A. S. P.*, **100**, 754.

Holtzman, J. A. 1990, *Pub. A. S. P.*, **102**, 806.

Howell, S. B., Mitchell, K. J., and Warnock, A. III 1988, *A. J.*, **95**, 247.

Howell, S. B. 1989, *Pub. A. S. P.*, **101**, 616.

Howell, S. B. 1990a, in *CCDs in Astronomy II: New Methods and Applications of CCD Technology,* ed. A. G. D. Philip, D. S. Hayes, and S. J. Adelman (Schenectady, NY: L. Davis Press), p. 133.

Howell, S. B. 1990b, in *CCDs in Astronomy,* ed. G. Jacoby, PASP Conference Series, Vol. 8, p. 312.

Howell, S. B. 1992, in *Astronomical CCD Observing and Reduction Techniques,* ed. S. B. Howell, PASP Conference Series, Vol. 23, p. 105.

Howell, S. B. 1993, in *Stellar Photometry,* ed. I. Elliat, Proc. of IAU Colloquium 136.

Howell, S. B. 1995, *Proc. of IAU Symposium 167, ed. A. G. D. Philip*, in press.

Howell, S. B. and Merline, W. J. 1995, *Proc. of IAU Symposium 167, ed. A. G. D. Philip*, in press.

Jacoby, G. H., ed. 1990, *CCDs in Astronomy,* PASP Conference Series, Vol. 8.

Jacoby, G. H., Ciardullo, R., and Ford, H. C. 1990, *Ap. J.*, **356**, 332.

Janesick, J. R., Hynecek, J., and Blouke, M. M. 1981, in *Solid State Imagers for Astronomy, Proc. SPIE,* **290**, 165.

Janesick, J., Elliot, T., Collins, S., Marsh, H., Blouke, M., and Freeman, J. 1984, in *Proc. SPIE,* Vol. 501.

Jayroe, R. R. 1984, *NASA Technical Paper 2396* .

Jayroe, R. R., and Schroeder, D. J. 1984, *NASA Technical Paper 2397* .

King, I. R. 1971, *Pub. A. S. P.*, **83**, 199.

King, I. R. 1983, *Pub. A. S. P.*, **95**, 163.

Kjeldsen, H., and Frandsen, S. 1992, *Pub. A. S. P.*, **104**, 413.

Massey, P. and Jacoby, G. H. 1992, in *Astronomical CCD Observing and Reduction Techniques,* ed. S. B. Howell, PASP Conference Series, Vol. 23, p. 240.

McMillan, R. S., and Stoll, C. P. 1982, in *Instrumentation in Astronomy IV, Proc. SPIE,* **331**, 104.

Mortara, L., and Fowler, A. 1981, in *Solid State Imagers for Astronomy, Proc. SPIE,* **290**, 28.

Nather, R. E. 1972, *Pub. A. S. P.*, **84**, 149.

Newberry, M. V. 1991, *Pub. A. S. P.*, **103**, 122.

Opal, C. B. 1988, in *Second Workshop on Improvements to Photometry,* ed. W. J. Borucki, NASA Conference Pub. 10015, p. 179.

Philip, A. G. D., Hayes, D. S., and Adelman S. J., ed. 1990, *CCDs in Astronomy II: New Methods and Applications of CCD Technology* (Schenectady, NY: L. Davis Press).

Press, W. H., Flannery, B. P., Teukolsky, S. A., and Vetterling, W. T. 1986, *Numerical Recipes, The Art of Scientific Computing* (Cambridge: Cambridge University Press).

Stetson, P. B. 1987, *Pub. A. S. P.*, **99**, 191.

Stetson, P. B. 1990a, *Pub. A. S. P.*, **102**, 932.

Stetson, P. 1990b, in *CCDs in Astronomy II: New Methods and Applications of CCD Technology,* ed. A. G. D. Philip, D. S. Hayes, and S. J. Adelman (Schenectady, NY: L. Davis Press), p. 71.

Stone, R. C. 1989, *A. J.*, **97**, 1227.

Young, A. T. 1974, *Ap. J.*, **189**, 587.

APPENDIX

Glossary of Parameters

a = area of obstruction by telescope secondary mirror

A = area of telescope primary mirror

A_0 = amplitude of PSF

$\bar{B}$ = average background level (ADU) [Background is distinguished from "sky" here because the background includes the DC bias and dark levels.]

c = speed of light

C = count rate of detected photons for source image (electrons/s/image)

d_1, d_2 = empirical fitting parameters for PSF

$\bar{d}$ = digitization offset (ADU)

$E(\lambda)$ = transmission of atmosphere as a function of wavelength

$\bar{E}$ = bandpass average of $E(\lambda)$

f = fractional count lost to digitization in a single pixel (ADU)

$\bar{f}$ = average value of f

f^* = f for a pixel in the source array (ADU)

f^B = f for a pixel in the background array (ADU)

$\bar{f}^*$ = average value of f^* (ADU)

$\bar{f}^B$ = average value of f^B (ADU)

$F(\lambda)$ = absolute flux from source, outside earth's atmosphere, as a function of wavelength (erg cm^{-2}s^{-1}Å^{-1})

$\bar{F}$ = bandpass average of $F(\lambda)$

G = gain of the CCD (electrons/ADU)

h = Planck's constant

i = subscript denoting pixel in source array

$I(x, y)$ = relative height of the PSF at rectangular coordinate x, y

$I(r)$ = relative height of the PSF at radial coordinate r

$I_i^\star$ = total counts on pixel i due to source only (ADU)

I_i^D = total counts on pixel i due to dark only (ADU)

I_i^S = total counts on pixel i due to sky only (ADU)

I_i^O = total counts recorded on pixel i due to DC bias only (ADU)

$I_i = I_i^\star + I_i^D + I_i^S + I_i^O$ = sum of all counts recorded on pixel i (ADU)

I_j^D = total counts on pixel j due to dark only (ADU)

I_j^S = total counts on pixel j due to sky only (ADU)

I_j^O = total counts on pixel j due to DC bias only (ADU)

$I_j = I_j^D + I_j^S + I_j^O$ = sum of all counts recorded on (background) pixel j (ADU) [Recall j refers to a pixel in the part of the grid selected for background determination.]

j = subscript denoting pixel in background array

n_B = number of pixels used in background (sky) determination

n_{pix} = number of pixels used in integration of source

$N_\star$ = total star counts (electrons)

N_S = total sky counts per pixel (electrons)

N_D = total dark count per pixel (electrons)

N_R = read noise (electrons/pixel/read) [used in Section 2H; $= \sigma_R$ in Section 2G]

p = empirical fitting parameter for PSF

p_{rx}, p_{ry} = empirical fitting parameters for PSF

p_r = empirical fitting parameter for PSF (here $p_r = p_{rx} = p_{ry}$)

$Q(\lambda)$ = quantum efficiency of CCD as a function of wavelength

$\bar{Q}$ = bandpass average of $Q(\lambda)$

r = radial distance from center of PSF

r_0 = radius (half-width at half maximum) of the PSF

r_x, r_y = radii of PSF along x, y directions

S = total, background corrected, signal from source (ADU)

$\bar{S}$ = mean value of S over many identical integrations

S/N = signal-to-noise ratio

$T(\lambda)$ = transmission of the filter as a function of wavelength

x, y = rectangular coordinates of a pixel or point in profile

$\epsilon(\lambda)$ = optical efficiency of telescope and instrument, without filter

$\bar{\epsilon}$ = bandpass average of $\epsilon(\lambda)$

λ = wavelength

λ_1, λ_2 = wavelength limits of bandpass

$\Delta\lambda = \lambda_2 - \lambda_1$ = width of bandpass

σ_R = the read noise associated with one read from a single pixel (electrons/pixel/read)

σ_X = standard deviation of the parameter X, where X is one of the parameters listed above